CD11B^{+}CD36^{+} cells are bone anabolic macrophages that limit age-associated bone loss

Short title: Age-associated cortical bone remodeling

Jinsha Koroth[1], Ismael Y. Karkache[1,2], Elizabeth K. Vu[1], Kim C. Mansky[2,3] and Elizabeth W. Bradley[1,4*]

1-Department of Orthopedic Surgery, University of Minnesota, Minnesota, United States of America

2-College of Veterinary Sciences, University of Minnesota, Minnesota, United States of America

3-School of Dentistry, University of Minnesota, Minnesota, United States of America

4-Stem Cell Institute, University of Minnesota, Minnesota, United States of America

*Corresponding author

E-mail address: ebradle1@umn.edu

Key words: bone, osteoclast, osteomac, bone remodeling, osteoclast progenitor, osteoprogenitor, osteoblast

ABSTRACT

Disruptions in the bone remodeling cycle that occur with increasing age lead to degeneration of the skeleton and increased risk of fragility fractures. Our understanding of how the bone remodeling process within cortical bone is controlled and altered with age in males and females is limited. Here, we generated bone marrow chimeric mice to understand the impacts of age and sex on the bone remodeling process. We demonstrate that transplantation of aged male or female bone marrow into young lethally irradiated male hosts unexpectedly enhances cortical bone mass without an impacting cancellous bone. Our single cell RNA-sequencing data show that mice reconstituted with aged bone marrow exhibited subsets of cells marked by CD11B/CD36 expression that demonstrate enhanced production of anabolic cytokines as compared to young counterparts, and that these myeloid subsets exist under conditions of normal physiology in aged mice. Importantly, $CD11B^{+}CD36^{+}$ cells do not differentiate into osteoclasts in vitro, and CD36 does not mark TRAP+ cells in vivo. Instead, $CD36^{+}$ cells localize to resorption sites, including within cortical bone defects, suggesting their involvement in cortical bone remodeling and healing. $CD11B^{+}CD36^{+}$ cells also express elevated levels of bone anabolic WNT ligands, especially Wnt6. In functional assays, we demonstrate that soluble factors produced by $CD11B^{+}CD36^{+}$ cells enhance osteoblast progenitor commitment, mineralization, and activation of WNT signaling in vitro. Moreover, CD11B/CD36 exquisitely mark a subset of anabolic myeloid cells within human bone marrow. In conclusion, our studies identified a novel population of aged macrophages that limit cortical bone loss.

INTRODUCTION

Bone mass in men and women starts to decline during the third decade of life (1). Women also exhibit a punctuated period of bone loss following the menopause proceeded by rate of age-associated declines in bone mass approaching that of men (2). In both men and women, age constitutes the greatest risk for a fragility fracture (3). Half of all women and one quarter of men are projected to suffer an age-related low bone mass fracture (4). Importantly, approximately 25% of individuals die a year after a hip fracture (5-9);

49 thus, a better understanding of the pathophysiology of age-related declines in bone mass would aid in
50 preventative and interventional strategies.

51 Cortical bone comprises the majority of skeletal bone mass (80%), and diminished cortical bone mass
52 accounts for 70% of bone lost with age (10, 11). Although bone anabolic agents enhance vertebral cortical
53 bone mass, efficacy is lower at the hip compared to the spine (+12.3% spine, +3.9% hip) (12, 13); therefore,
54 additional therapeutics improving cortical bone are desperately needed.

55 The bone remodeling process facilitates homeostasis of the adult skeleton. Bone remodeling consists of
56 phases of activation, bone resorption, reversal, and bone formation (14). Aging disrupts the phases of the
57 bone remodeling process resulting in unbalanced bone formation and bone resorption (14). Osteoclasts
58 and osteoblasts mediate these phases, respectively. While the coupled cellular activities of osteoclasts
59 and osteoblasts maintain optimal bone health, recent evidence suggests that macrophages within the
60 bone niche help coordinate the bone remodeling process (14). In spite of this, we understand little about
61 how different subsets of macrophages impact the bone remodeling process. In this study, we sought to
62 define how age affects macrophage types and examine the impact of those cells on cortical and trabecular
63 bone homeostasis.

64 **RESULTS**

65 **Transplantation of aged bone marrow into young hosts promotes cortical bone mass**

66 Recent work supports that myeloid cells residing within the bone marrow regulate bone remodeling
67 during conditions of normal physiology and pathological conditions (15, 16). Lower peak bone mass and
68 acute bone loss following the menopause predisposes women to osteoporosis and greater risk of fracture
69 with age; however, it is unclear if rapid bone loss associated with sex steroid deficiency and age-associated
70 bone loss are mediated by the same mechanisms, or if there are differences in how age-associated bone
71 loss occurs in males and females. To understand the cellular mechanisms driving bone loss prior to

72 reproductive senescence, we performed bone marrow transplantation assays generating chimeric mice.
73 We started with young (e.g., 6-week-old) male recipient mice (Figure 1A, left panel). Young recipient male
74 mice were lethally irradiated to ablate the bone marrow. In parallel, we collected bone marrow from 6-
75 or 40-week-old donor male or female mice (Figure 1A, right panel). Donor bone marrow was depleted of
76 T cells through magnetic-assisted cell sorting (MACS)-mediated removal of CD3+ and CD8+ cells. Young
77 recipient mice were then reconstituted with T-cell depleted donor bone marrow from mice of four groups
78 (Figure 1A, right panel) (17-19). We then aged recipient male mice to six-months (e.g., 18-weeks after BM
79 transplantation). To estimate percent chimerism, we collected bone marrow and liver cells from male
80 recipient mice transplanted with female bone marrow, and assessed expression of X- and Y-linked genes.
81 Within the bone marrow, male recipient mice showed robust expression of X-linked genes Xist and Gata1,
82 but little to no expression of Y-linked genes Sry and DDx3y (Figure 1B), supporting that cells within the
83 bone marrow of ablated recipient males were reconstituted by female cells. In contrast, X- and Y-linked
84 genes were expressed within the male recipient liver. Gross examination showed that male mice receiving
85 bone marrow from either aged males (group 2) or aged females (group 4) exhibited signs of premature
86 aging (e.g., gray coat color) (Figure 1C). Body weight was also reduced by transplantation of aged male
87 bone marrow (e.g., group 2), but no other significant weight changes were observed (Figure 1D).
88 Splenomegaly can point to deficiencies in bone marrow function, so we also assessed the spleen weight
89 to body weight ratio. Changes in body weight-adjusted spleen mass were not observed within any group
90 (Figure 1E).

91 We next assessed bone mass of 24-week-old recipient male mice. We first determined how irradiation
92 affected cortical bone by comparing chimeric mice within each group to 24-week-old non-irradiated
93 controls. We noted that irradiation decreased cortical BV/TV (Figure 2A, D), but did not alter cortical
94 thickness (Figure 2B, D) or trabecular BV/TV (Figure 2D, E) when comparing non-irradiated controls to
95 male mice transplanted with sex- and age-matched bone marrow (e.g., group 1 vs NI). Likewise, enodsteal

96 perimeter was significantly increased when comparing to non-irradiated controls (Figure 2C). In contrast,
97 irradiation increased trabecular spacing but reduced trabecular thickness (Figure 2D, F, G).

98 We next assessed changes between groups 1 and 2 to determine the effect that aged, but sex-matched
99 bone marrow had on cortical and trabecular bone. Micro-CT analyses of the resulting chimeric mice in
100 groups 1 and 2 revealed a surprising increase cortical bone mass (+10%) and cortical thickness (+7%) when
101 male recipients were reconstituted with sex-matched, but aged bone marrow (Figure 2A, B, D). In
102 contrast, no changes in trabecular BV/TV were observed between these groups (Figure 2D, E), but we did
103 note increased trabecular spacing coupled with diminished trabecular thickness (Figure 2D, F, G). These
104 data suggested that transplantation of aged bone marrow enhanced cortical but not trabecular bone
105 mass.

106 We next examined the effects transplantation of bone marrow derived from female mice on bone mass.
107 When comparing young male mice reconstituted with bone marrow from age-matched males or females
108 (groups 1 and 3), we did not see a change in cortical BV/TV or cortical thickness (Figure 2A, B, D). Likewise,
109 trabecular BV/TV, trabecular number, and trabecular spacing were unchanged (Figure 2D-F), but we did
110 observe a slight reduction in trabecular thickness when comparing these groups (Figure 2G).

111 We next compared young male mice transplanted with either sex- and age-matched bone marrow to
112 those transplanted with bone marrow collected from 40-week-old females (groups 1 and 4). We noted
113 increased cortical BV/TV, but no significant changes in cortical thickness (Figure 2A, B, D). No changes in
114 trabecular bone parameters were noted (Figure 2D-G). We then compared the effects of age when
115 transplanting female bone marrow (e.g., groups 3 versus 4). Reconstitution of young male mice with aged
116 female bone marrow enhanced cortical BV/TV as compared to age-matched female bone marrow, but did
117 not alter cortical thickness (Figure 2A, B, D). No changes in trabecular BV/TV, trabecular number, or
118 trabecular spacing were noted (Figure 2D-F), but we did observe an increase in trabecular thickness

119 (Figure 2G). These results mirror those we observed when aged male bone marrow was transplanted into
120 young male recipients.

121 Enhanced cortical bone mass could be due to increased bone formation and/or a reduction in bone
122 resorption at the periosteal or endosteal surfaces, respectively. To determine how bone remodeling was
123 altered within our chimeric mice we examined periosteal and endosteal cortical bone perimeter.
124 Irradiation increased endosteal perimeter when comparing mice within group 1 to non-irradiated
125 controls, supporting that irradiation increases resorption at the endosteal surface. In contrast, mice
126 transplanted with aged bone marrow within group 2 exhibited decreased endosteal perimeter (Figure 2C).
127 Likewise, transplantation of female bone marrow diminished endosteal perimeter (Figure 2C). These
128 results suggest that transplantation of aged bone marrow reduced endosteal resorption of cortical bone
129 or lead to increased endosteal formation.

130 **Subsets of myeloid cells from aged bone marrow associate with enhanced cortical bone**

131 Our results from the bone marrow transplantation assays combined with recent work demonstrating that
132 myeloid lineage cells (e.g., erythromyeloid progenitors, osteoclasts, osteomorphs, osteomacs) regulate
133 the bone remodeling process, suggested the existence of aged myeloid cells that promote maintenance
134 of cortical, but not trabecular bone. Moreover, a recent study demonstrated that erythromyeloid
135 progenitors expand during intensive hematopoietic regeneration (20); therefore, we profiled myeloid
136 cells within the bone marrow of our chimeric mice. We first evaluated the cellular subsets in young male
137 recipients transplanted with sex-matched bone marrow derived from either age-matched or 40-week-old
138 mice via singe cell RNA-sequencing (scRNA-Seq) of $CD11B^{+}$ cells. Integration of these two datasets did not
139 uncover unique clusters (Figure 3A), but we noted differential gene expression within clusters when
140 comparing CD11B+ cells from mice reconstituted with aged as compared to age-matched bone marrow
141 from either males (Figure 3) or females (Figure 4).

142 In mice reconstituted with male cells, all clusters expressed markers for hematopoietic cells, including
143 *Cd45*, *Pu.1* and *Chi3l* (Figure 3B-D). We also noted multiple *Csf1r*$^{+}$ clusters, including clusters 1, 4, 7, 8, 14,
144 15, and 16 (Figure 3E, R). Expression of *Kit* and *Myb* marked highly proliferative cells within clusters 6 and
145 12, which are likely myeloid progenitor cells (Figure 3F, G). Macrophage markers *F4/80*, *Cd68*, and *Cd86*
146 were likewise expressed by cells within clusters 1, 4, 7, 8, and 14-16 (Figure 3H-J). The putative osteomac
147 marker *Cd166* (21) was broadly expressed (Figure 3K), whereas the macrophage marker *Mrc1* was mostly
148 restricted to clusters 14-16 (Figure 3L, R). Cells within cluster 16 expressed the highest levels of *Mrc1*, but
149 expression was diminished by cells within cluster 15 (Figure 3L, R). Similarly, expression of *Cx3cr1* was
150 restricted to clusters 14-16, with highest expression observed by cells within cluster 15 (Figure 3M, R).
151 Some cells within cluster 14-16 also expressed *RANK* (Figure 3N), supporting the role of these cells as with
152 the potential to give rise to osteoclasts. We also noted high enrichment of *Cd74*, a putative osteomorph
153 marker (22), *Siglec1/Cd169*, and *Cd36* within clusters 14-16 (Figure 3O-R). Recent genetic evidence
154 suggests that cortical bone may be controlled specifically by several signaling pathways/components (e.g.,
155 Wnt and Notch signaling) (23). We next evaluated expression of these and related genes across all clusters
156 and noted high expression of Bmps, Collagens, and Wnts by cells within clusters 14-16, and to some extent
157 cluster 17 (Figure 2R). Enrichment of B Cell markers distinguished cluster 17.

158 We next evaluated the effect of sex on subsets of CD11B^{+} cells following intensive bone marrow
159 reconstitution. We integrated scRNA-Seq results from the CD11B^{+} cells within the bone marrow of young
160 male mice reconstituted with either age-matched male bone marrow or 40-week-old female bone
161 marrow. This analysis did not reveal unique clusters (Figure 4A). As above, *Cd45*, *Pu.1*, and *Chi3l* were
162 broadly distributed (Figure 4B-D). *Csf1r*+ clusters included clusters 1- 3, 11, 12, 15 and 17 (Figure 4E).
163 Myeloid progenitor cells marked by expression of *Kit* and *Myb* were contained within 6 and 9 (Figure 4F,
164 G). The cells within clusters 1-3, 5, 11, 12, 15, and 17 expressed the macrophage markers *F4/80*, *Cd68*,
165 and *Cd86* (Figure 4H-J); *Cd166* was broadly expressed (Figure 4K). In contrast, *Mrc1* was expressed by

166 cells within clusters 12 and 17 (Figure 4J, R). High expression of *Cx3cr1* marked cells within clusters 11 and
167 15, whereas expression was diminished with clusters 12 and 17 (Figure 4M, R). Expression of RANK was
168 observed by cells within clusters 11 and 15-17 (Figure 4N). High expression of *Cd74* was also noted of
169 clusters 11, 12 and 15-17 (Figure 4O, R), whereas *Cd36* was localized to cells within clusters 11, 12, 17 and
170 15, with cluster 11 exhibiting lower expression (Figure 4Q, R). As above, we noted enriched expression of
171 Bmps, Collagens, and Wnts by cells within clusters 12, 15 and 17 (Figure 4R). We observed similar findings
172 when comparing CD11B$^+$ cells from young male mice reconstituted with bone marrow from 40-week-old
173 males to those reconstituted with 40-week-old females, demonstrating that age, but not sex of donor
174 cells associated with enhanced cortical bone mass. Likewise, our data suggest that specific subsets of
175 CD11B+ cells express bone anabolic genes, and that these subsets are delineated by differential
176 expression of *Cd36*.

177 **Characterization of CD11B$^+$ cellular subsets within the bone marrow of young and aged animals**

178 We noted the presence of several cellular subsets of cells within aged mice that expressed bone anabolic
179 genes. To broadly define the types of myeloid cells within the bone marrow and evaluate how age alters
180 these cellular subsets, we performed single cell RNA-sequencing (scRNA-Seq) on CD11B$^+$ cells from the
181 bone marrow of 8- or 40-week-old male and female C57Bl6/J mice. We chose these ages to reflect a period
182 of bone anabolism (e.g., gain in bone mass) during youth and a period of age-associated bone loss prior
183 to reproductive senescence, respectively. scRNA-Seq of CD11B$^+$ cells from young animals revealed
184 multiple cells types, including *RANK*$^+$ osteoclast progenitors, dendritic cells, neutrophils, monocytes,
185 macrophages as well as proliferative *Kit*$^+$/*Myb*$^+$ myeloid progenitors (Figure 5A, C).

186 We first examined macrophage clusters within young males and females. We noted two macrophage
187 clusters within 8-week-old CD11B-expressing bone marrow cells. Cluster 8 exhibited reduced expression
188 of *Csf1r*, *Cx3cr1* and *Cd74*, but higher expression of *Mrc1* and *Cd36* (Figure 5B). Cluster 8 showed
189 enrichment in bone anabolic genes such as BMPs, Collagens and Wnts. These bone anabolic proteins

190 were also expressed by *Csf1r*- cells within cluster 11. Likewise, we identified three *Csf1r*-expressing
191 clusters within CD11B$^+$ cells derived from the bone marrow of 8-week-old females (Clusters 3, 4, and 6,
192 Figure 5C, D). Clusters 3 and 6 demonstrated reduced expression of *Csf1r*, but levels of *Mrc1* and *Cd36*
193 were greater (Figure 5D). Cluster 4 demonstrated the highest enrichment for *Csf1r* and *Cx3cr1*, but
194 exhibited little expression of *Cd36* or *Cd74*. Bone anabolic genes were enriched in clusters 3 and 6 (Figure
195 5D). These data pointed to a set of macrophages within the bone marrow that produce bone anabolic
196 factors.

197 When examining aged CD11B$^+$ cells, we likewise noted several myeloid subsets that were analogous to
198 those present within young animals. Within males, we noted three subsets (clusters 4, 9, and 10) that all
199 showed enrichment for *Csf1r* and *Cx3cr1* (Figure 5E, F). Moreover, clusters 9 and 10 demonstrated high
200 expression of *Cd36*, but enrichment in *Cd74* by cells within cluster 9 and *Mrc1* by cells in cluster 10
201 differentiated these clusters (Figure 5F). All three clusters exhibited enrichment in Wnt gene expression,
202 but only clusters 9 and 10 significantly expressed Bmps. Within CD11B$^+$ female ages cells, clusters 7, 8, 9,
203 and 14 all showed enrichment for *Csf1r*, *Mrc1* and *Cd36* (Figure 5G, H). *Cx3cr1* expression defined cluster
204 7 as well as cluster 9, but to a much lesser extent. *Cd74* also demonstrated differential expression
205 amongst these four clusters (Figure 5H). Cluster 7 showed limited expression of Bmps and Wnts, whereas
206 these bone anabolic genes were enriched amongst clusters 8, 9, and 14 (Figure 5H). These data highlight
207 subsets of CD11B$^+$/*Csf1r*$^+$ cells within the bone marrow of aged animals that can be delineated by
208 differential expression of *Cd74*, *Cx3cr1*, *Mrc1*, and/or *Cd36*.

209 **CD36+ cells associate with sites of bone resorption on endocortical surfaces**

210 *Cd36* represented one of the most highly differentially expressed genes in our scRNA-Seq analyses and
211 was exclusively expressed by specific subsets of cells within our analyses. We postulated that
212 CD11B$^+$CD36$^+$ cells either serve as osteoclast progenitors, or play a regulatory role in the bone remodeling

213 process given that they are enriched in chimeric mice with elevated cortical bone mass. To investigate
214 their localization and potential function, we performed immunohistochemical (IHC) staining for CD36 on
215 femur sections from 12- and 24-week-old female mice. We also examined sections of cortical bone defects
216 collected 14 days post-injury (24). To visualize bone remodeling sites, we additionally performed TRAP
217 staining. Our results showed that CD36 was diffusely expressed by cells within the BM cavity, with no
218 enrichment near cortical bone remodeling sites in 12-week-old female mice (Figure 6A, left column).
219 However, in 24-week-old mice and within cortical bone defects, we observed strong CD36 staining in cells
220 located near osteoclasts (Figure 6A, middle and right columns). CD36 expression by mature osteoclasts
221 was not detected under any conditions. These results suggest that $CD36^{HI+}$ cells may regulate bone
222 remodeling and regeneration.

223 To assess whether CD11B+CD36+ cells function as osteoclast progenitors, we isolated $CD11B^{+}CD36^{+}$ and
224 $CD11B^{+}CD36^{-}$ cells from the BM of 12-week-old female mice and cultured them under osteoclastogenic
225 conditions. While the $CD11B^{+}CD36^{-}$ population formed $TRAP^{+}$ multinucleated cells, indicative of
226 osteoclasts, the $CD11B^{+}CD36^{+}$ cultures only produced mononuclear cells (Figure 6B, lower panel). These
227 findings suggest that $CD11B^{+}CD36^{+}$ cells are involved in cortical bone regeneration and remodeling but do
228 not form osteoclasts, supporting previous reports (25).

229 **$CD11B^{+}CD36^{+}$ myeloid cells support bone formation**

230 Our scRNA-Seq analysis revealed that $CD11B^{+}CD36^{+}$ cells express several bone anabolic factors, including
231 *Wnt10b*, *Wnt6*, *Wnt3a*, *Bmp1*, and *Bmp2* (Figure 3R). To validate these findings, we FACS-sorted
232 $CD11B^{+}CD36^{+}$ cells from the bone marrow of 12-week-old female mice. $CD11B^{+}CD36^{+}$ cells comprised
233 8.7% of the isolated bone marrow cells (Figure 7A). We observed increased expression of *Wnt10b*, *Wnt6*,
234 and *Bmp1*, and reduced expression of *Wnt3a* and *Bmp2* by $CD11B^{+}CD36^{+}$ cells compared to $CD11B^{+}CD36^{-}$

235 cells (Figure 7B-F). *Wnt6* showed the most significant differential expression, which we further confirmed
236 by western blotting (Figure 7G).
237
238 Next, we investigated whether factors secreted by CD11B$^+$CD36$^+$ cells influence osteoprogenitor
239 proliferation, migration, commitment, and mineralization. CD11B$^+$CD36$^-$ and CD11B$^+$CD36$^+$ cells were
240 sorted from the BM of 12-week-old male and female C57Bl/J mice, cultured with M-CSF for three days,
241 and conditioned medium was collected. ST2 osteoprogenitor cells were then cultured in conditioned
242 medium for 24 hours to assess proliferation and migration (Figure 7H). Cck-8 assays indicated no
243 significant impact on osteoprogenitor proliferation and transwell assays similarly showed no significant
244 effects on migration. To evaluate osteoprogenitor commitment and mineralization, ST2 cells were
245 cultured in conditioned medium under osteogenic conditions. Enhanced mineralization was observed in
246 cultures treated with CD11B$^+$CD36$^+$ conditioned medium (Figure 7K, L) accompanied by increased
247 expression of *Bgn*, *Phospho1*, and *Sp7* (Figure 7M-O). Conversely, *Mmp13* and *Tnfsf11*/RANKL expression
248 was reduced in these cultures (Figure 7P, Q). Finally, we assessed the activation of β-catenin and JNK
249 signaling pathways in ST2 cells cultured in conditioned medium from CD11B$^+$CD36$^-$ and CD11B$^+$CD36$^+$ cells
250 for one hour. Western blotting revealed elevated levels of active β-catenin and JNK phosphorylation,
251 indicating increased canonical and/or non-canonical Wnt signaling (Figure 7R). Likewise, NFAT1 and
252 TCF1/7 levels were enhanced (Figure 7R). These results suggest that CD11B$^+$CD36$^+$ cells produce WNT6,
253 which promotes osteoblast differentiation and bone formation.

254 **CD11B$^+$CD36$^+$ Cells within Human Bone Marrow**

255 To show that our results may translate to humans, performed single cell sequencing of CD11B$^+$ cells from
256 the bone marrow aspirate of a 45-year-old female. Using the pipeline described above, we aligned data
257 to the hg38 genomic reference genome. We identified a cluster of isolated CD11B$^+$ cells exquisitely
258 defined by *Cd36* (Figure 8A, Q, R). CD11B$^+$CD36$^+$ cells within cluster 7 also expressed *Cd45*, *Pu.1*, *Csf1r*,

259 *F4/80*, *Cd68*, *Cd86*, *Cd166*, *Cd74*, and *Cx3cr1*, but were mostly negative for *Chi31l*, *Mrc1*, *RANK*, and
260 *Siglec1/Cd169* (Figure 8B-P). We also noted that expression of *Cd166*, the putative osteomac marker, and
261 *Cd74* were broadly pressed by CD11B$^+$ cells (Figure 8K, O). Expression of *Wnt6* was likewise restricted to
262 CD11B$^+$ cells cluster 7; thus, bone marrow from aged humans also contains an anabolic macrophage
263 population marked by CD11B/CD36.

264 **DISUCSSION**

265 The goal of our study was to examine how age and sex of hematopoietic cells affected skeletal aging. Prior
266 work documented that altered mesenchymal cell function facilitates age-associated changes to trabecular
267 bone, with consequent myeloid cell skewing (26, 27). Our study supports this finding, as we did not
268 observe changes to trabecular bone mass or microarchitecture. In contrast, our data support that age
269 alters bone marrow composition following intensive hematopoietic regeneration as previously described
270 (20), and those alterations in bone marrow composition facilitate gains in cortical bone. Moreover, our
271 data suggest that a subpopulation of aged macrophages limit endocortical bone resorption.

272 Bone resorbing osteoclasts can arise from hematopoietic stem cells or from long-lived erythro-myeloid
273 progenitors within the bone marrow. Osteoclasts have an estimated 6-month half-life in mice (28-30).
274 Recent evidence suggests that osteoclasts derived from different subsets of progenitors may facilitate
275 bone remodeling in different contexts (31-33). For instance, osteoclast progenitors that contribute to
276 homeostatic bone remodeling differ from those mediating bone loss associated with inflammatory
277 conditions (32). Osteoclasts that remodel bone in other perturbed states or within different bone
278 compartments may likewise differ. Our data suggest that age-associated resorption at endosteal cortical
279 bone surfaces may be distinct and limited by secreted factors produced CD11B$^+$CD36$^+$ cells. To the best of
280 our knowledge, this represent the first example of an aged myeloid cell type that limits bone resorption.

281 In our study, we identified a specific myeloid subset of aged cells that limit age-associated cortical bone
282 loss. Surface marker expression of CD11B and CD36 characterizes this subset of cells. In addition to these
283 surface markers, osteomorph markers (e.g., Axl, Cadm1, Ccr3, Cd74, Vcam1 (22)) were significantly
284 enriched within our identified myeloid subset. Osteomorphs have be speculated to function during the
285 reversal phase of bone remodeling. Given their proximity to bone resorbing osteoclasts along the cortical
286 surface, our identified cellular subset could be osteomorphs. Indeed, our scRNA-Seq analyses
287 demonstrated expression of RANK within these clusters, but we were unable to generate osteoclasts from
288 sorted $CD11B^{+}CD36^{+}$ cells in vitro. In contrast, $CD11B^{+}CD36^{-}$ cells efficiently formed osteoclasts in vitro.
289 These data suggest that our identified myeloid subset is potentially distinct from osteomorphs, but we do
290 not know if $CD11B^{+}CD36^{+}$ cells could fuse with existing osteoclasts in vivo.

291 CD36 is a cell surface marker delineating our population of interest, but we are unsure if CD36 is merely
292 a marker for this myeloid subset, or if CD36 plays a functional role in controlling age-associated cortical
293 bone loss. CD36 is a membrane glycoprotein that functions as a scavenger receptor for various ligands,
294 including collagen, thrombospondin-1, anionic phospholipids, and long chain fatty acids. While CD36 is
295 broadly expressed, adipocytes, cardiac myocytes, and immune cells including myeloid cell types (e.g.,
296 monocytes, macrophages) exhibit biased expression. CD36 mediates the formation of giant cells, but does
297 not facilitate osteoclast fusion (25). Our data further confirm that $CD11B^{+}CD36^{+}$ cells do not form
298 osteoclasts.

299 Global deletion of *Cd36* (i.e., *Cd36*$^{-/-}$) resulted in conflicting effects on bone mass. In the first published
300 study, male and female 1- to 6-month-old *Cd36*$^{-/-}$ mice demonstrated reduced vertebral and femoral
301 cortical bone mass characterized by diminished bone formation (34). No changes in markers of resorption
302 were noted (34). Furthermore, in vitro osteoblastogenesis from bone marrow stromal cells was
303 diminished, though the impact of myeloid cell *Cd36* deletion in these cultures could be a confounding
304 factor. Conversely, a later study reported increased vertebral and femoral cortical BV/TV in female 12-

305 week-old *Cd36*$^{-/-}$ mice, with no detection of CD36 expression by mature osteoclasts or osteoblasts (35).
306 Given these conflicting results using *Cd36* global knockout mice, an examination of the role of *Cd36*
307 specifically within monocyte/macrophage-lineage cells during bone remodeling and regeneration is
308 warranted as understanding the role of *Cd36* in bone biology would offer potential therapeutic targets for
309 managing bone-related diseases and improving skeletal health.

310 Our scRNA-Seq data demonstrated enrichment of secreted factors (e.g., Wnts, Bmps) by aged myeloid
311 cells within our clusters of interest. Coupled with decreased endosteal perimeter, we speculated that
312 CD11B^{+}CD36^{+} cells may limit resorption at endosteal surfaces. Wnt signaling limits osteoclastogenesis
313 (36). Likewise, canonical Wnt signaling promotes expression of OPG by osteoblasts, leading to diminished
314 osteoclastogenesis (37). In contrast, little is known about production of Wnt ligands by other cell types
315 involved in the bone remodeling process and how this impacts cortical bone resorption. In fact, studies
316 suggest that osteoclasts and bone forming osteoblasts may not be present at sites of bone remodeling at
317 the same time (38-40), particularly at the endosteal surface. Likewise, age disrupts the temporal and
318 spatial processes of resorption and formation. Our studies point to CD11D^{+}CD36^{+} cells as targets to limit
319 age-associated cortical bone loss. In future studies, we will determine factors produced CD11B^{+} CD36^{+}
320 cells that limit age-associated osteoclastogenesis and bone resorption.

321 Our study has several limitations. One limitation of our study is that we did not assess possible
322 contributions of splenic cells to our phenotype. Studies have shown that osteoclast progenitors from the
323 spleen can migrate to bone and participate in bone remodeling and repair (28, 31, 33). We did not observe
324 significant expression of X-linked gene within the bone marrow of males reconstituted with female bone
325 marrow or splenomegaly; nonetheless, we cannot completely rule out the contribution of these cells
326 within our study. Although we speculate that CD11B^{+}CD36^{+} cells are not osteomorphs based on their
327 inability to support osteoclastogenesis in vitro, we do not know if this is true in vivo. Our definition of aged
328 mice does not strictly fit the well-accepted definition (e.g., older than one year). We wanted to uncover

329 mechanisms of age-associated bone loss independent of reproductive status to reflect what may be
330 initiating events in the aging process as both men and women begin to lose bone mass starting in the third
331 decade of life.

332 **MATERIALS AND METHODS**

333 *Animal procurement and housing*

334 The Jackson Laboratory provided male and female C57Bl6/J mice (strain #000664, Bar Harbor, ME, USA)
335 aged to either 6- or 38-weeks old at time of purchase. Mice were acclimated to housing conditions for
336 two weeks prior to experimentation. All animal research was conducted according to guidelines provided
337 by the National Institutes of Health and the Institute of Laboratory Animal Resources, National Research
338 Council. The University of Minnesota Institutional Animal Care and Use Committee approved all animal
339 studies.

340 *T Cell Depletion of Whole Bone Marrow*

341 Male and female 8- or 40-week-old mice were euthanized by CO_2 asphyxiation. The femora and tibiae
342 were collected and connective tissue was removed. Bone epiphyses were removed and the marrow cavity
343 was flushed with sterile PBS. Whole bone marrow suspensions from age-matched mice were pooled and
344 pelleted at 1000 rpm for five minutes. Cell pellets were then suspended in 1X RBC lysis buffer (#00-4333-
345 57, ThermoFisher Scietific, Waltham, MA, USA) and incubated for five minutes. Cells were pelleted at 1000
346 rpm and suspended in MACS buffer (0.5% bovine serum albumin, 2mM EDTA, phosphate buffered saline)
347 by diluting MACS BSA stock solution (Miletnyi Biotech, Bergisch Gladbach, North Rhine-
348 Westphalia, Germany, #130-091-376) 1:20 with autoMACS rinsing solution (Miltenyi Biotech, #130-091-
349 222,) to a density of $0.2x10^6$ cells/µl. Cell suspensions were then incubated with 1 µl PE-conjugated anti-
350 Cluster of CD8 and anti-CD3 antibodies per $1x10^7$ nucleated cells for 20 minutes in the dark at 4C. Cells
351 were then washed with MACS buffer, pelleted and suspended at a density of 1.25x106 cells/µl in MACS
352 buffer. Anti-PE microbeads (20 µl/$10x10^6$ cells, Miltenyi Biotech, #130-048-801) were added and cells

353 were incubated at 4C for 20 minutes in the dark. Cells were then washed pelleted and applied to an LS
354 column (#130-042-401, Miltenyi Biotech) placed in a MidiMACS Separator magnet (Miltenyi Biotec, #130-
355 042-301h). Eluted $CD8^-/CD3^-$ bone marrow cells were pelleted and suspended in PBS at a density of $50x10^6$
356 cells/ml.

357 *Irradiation and bone marrow reconstitution*

358 Six-week-old (e.g., young) male mice (n=34) were lethally irradiated using and X-ray irradiator via two
359 successive does of 500 rads separated by a period of four hours. Two hours after completion of irradiation,
360 mice were reconstituted via a 200 µl tail vein injection of $10x10^6$ T cell-depleted whole bone marrow cells
361 suspended in PBS derived from either 6-week-old males (n=10), 6-week-old females (n=8), 40-week-old
362 males (n=8), or 40-week-old females (n=8). Following bone marrow reconstitution, mice were housed in
363 autoclaved cages and were administered 15 µg polymixin B sulfate and 40 µg/ml neomycin sulfate in their
364 drinking water for two weeks. Mice were aged an additional 16 weeks (e.g., 24-weeks-old) and then
365 euthanized for analyses.

366 *Micro-computed tomography*

367 Right femora collected from 24-week-old chimeric mice and non-irradiated 24-week old males were fixed
368 in 10% neutral buffered formalin for 48 hours, wrapped in gauze, and placed in 1.5mL screw-cap tubes
369 filled with 70% ethanol. Scanning was performed using the XT H 225 micro-computed tomography (micro-
370 CT) machine (Nikon Metrology Inc., Brighton, MI, USA) set to 120kV, 61µA, 720 projections at two frames
371 per projection with an integration time of 708 milliseconds as previously described (41). Scans were done
372 at an isometric voxel size of 7.11 µm with a 1mm aluminum filter, 17 minutes per scan. Each scan volume
373 was reconstructed using CT Pro 3D (Nikon metrology, Inc., Brighton, MI, USA). Reconstructions were
374 converted to bitmap datasets using VGStudio MAX 3.2 (Volume Graphics GmbH, Heidelberg, Germany).
375 Scans were reoriented via DataViewer (SkyScan, Bruker micro-CT, Belgium) to create a new bitmap
376 dataset for consistent analysis. From these data, representative transverse slices were selected for

377 qualitative analysis. Morphometric analysis was performed using SkyScan CT-Analyzer (CTAn, Bruker
378 micro-CT). Bruker's instructions and guidelines for analysis within the field was followed throughout
379 analysis (41). 3D Analysis of trabecular bone was performed in the distal metaphysis 0.7 mm proximal to
380 the growth plate and extending 1.5 mm proximally toward the bone diaphysis. For the bone cortex, 2D
381 analysis occurred in a 0.5 mm section within the mid-diaphysis defined as 4 mm from the growth plate.
382 Regions of interest were set by automated contouring for the trabecular and cortical ranges, with some
383 manual editing when necessary. Binary selection of all samples resulted in two separate global thresholds
384 used to separate bone from surrounding tissue within the trabecular and cortical regions of interest.
385 Parameters measured for trabecular bone include bone volume per total volume (BV/TV), bone surface
386 per total volume (BS/TV), bone surface per bone volume (BS/BV) trabecular thickness, number, and
387 spacing (Tb.Th, Tb.N, Tb.Sp), and connective density (Conn.D). Cortical parameters measured were BV/TV,
388 periosteal and endosteal perimeter (pM), as well as cortical thickness (Ct.Th).

389 *CD11B$^+$ magnetic assisted cell sorting*

390 Bone marrow cells were flushed from the femora and tibiae of 6-month-old chimeric mice from each
391 group or from 8- and 40-week-old male and female C57Bl6/J mice. Whole bone marrow suspensions
392 resulting from each mouse were pelleted at 1000 rpm for five minutes. Cell pellets were then suspended
393 in 1X RBC lysis buffer and incubated for five minutes. Cells were pelleted at 1000 rpm and suspended in
394 MACS buffer to a density of 0.11×10^6 cells/µl. Nucleated cells were then incubated with 10 µl CD11B
395 microbeads (Miltenyi Biotech, #130-126-725) per 1×10^7 cells for 10 minutes at 4C. Cell suspensions were
396 then brought to a total volume of 500 µl with MACS buffer and applied to an equilibrated LS column placed
397 in a MidiMACS Separator magnet. Columns were then washed three times with MACS buffer and removed
398 from the magnet. CD11B$^+$ cells were eluted from the column with 5 ml MACS buffer. Cells were then
399 enumerated and used for subsequent scRNA-Seq analyses.

400 *Single cell RNA-sequencing*

401 CD11B+ cells from chimeric mice in each group or 8- and 40-week-old male and female C57Bl6/J mice
402 were isolated via MACS as described above. Single cell cDNA libraries from each sample were the
403 prepared using Chromium Single cell 3' Reagent v3 Kits (10× Genomics, Pleasanton, CA, USA) according to
404 the manufacturer's protocol. Each single-cell suspension was mixed with primers, enzymes, and gel beads
405 containing barcode information and then loaded on a Chromium Single Cell Controller (10× Genomics) to
406 generate single-cell gel beads in emulsions (GEMs). Each gel bead was bonded to one cell and encased
407 within oil surfactant. After generating the GEMs, reverse transcription was performed using barcoded full-
408 length cDNA followed by the disruption of emulsions using the recovery agent and cDNA clean up with
409 DynaBeads MyOne Silane Beads (ThermoFisher Scientific, #37002D). cDNA was then amplified by PCR
410 with an appropriate number of cycles and thermal conditions that depended on the recovery cells.
411 Subsequently, the amplified cDNA was fragmented, end-repaired, A-tailed, ligated to an index adaptor,
412 and subjected to library amplification. Quality of amplified cDNA was assessed using an Agilent
413 Bioanalyzer prior to high-throughput sequencing. Following quality control, the cDNA libraries were
414 sequenced on an Illumina NovaSeq 6000 sequencer. The Genomics Core at the University of Minnesota
415 performed library construction and sequencing.

416 *Single Cell Bioinformatic Analyses*

417 10× Genomics Cell Ranger software (version 6.0.0) was used to process the raw scRNA-seq data in
418 accordance with the guidelines specified by the manufacturer. Cell Ranger software (2020-A, 10×
419 Genomics Cell Ranger Count v7.0.1) was used to demultiplex the raw base call (BCL) files produced by the
420 Illumina NovaSeq 6000 sequencer. Next, Cell Ranger was used to count the unique molecular identifiers
421 (UMI) and barcodes and align fastq files to the mouse reference genome (GRCm39). Quality assurance
422 and subsequent studies were then performed on the feature-barcode matrices created by Cell Ranger.
423 The study was filtered to exclude cells with outlier status, aberrant gene detection rates (<500 and
424 >5,000), and high mitochondrial transcript level (>8%), a sign of cellular stress. Possible doublets were also

425 excluded from the data using doubletFinder for subsequent analysis. The remaining cells are then
426 normalized, and a set of 2000 highly variable genes were selected based on a variance stabilizing
427 transformation ('vst'). Next, the data was scaled to account for technical variability in the data and used
428 for principal component analysis (PCA) to reduce the dimensionality of the data. Cells were then organized
429 into an ideal number of clusters for de novo cell type discovery. Then, using uniform manifold
430 approximation and projection (UMAP), a non-linear dimensional reduction was carried out, enabling for
431 the identification and visualization of different cell clusters. After variable feature identification, the data
432 were used for integrated analysis.

433 *$CD11B^+CD36^+$ Cell Isolation*

434 Whole bone marrow was flushed from the hind limbs of 6-8-week-old male and female C57Bl6/J mice
435 (n=3 per sex) and red blood cells were lysed with 1X RBC lysis buffer as described above. Nucleated cells
436 from whole bone marrow were pelleted at 1000 rpm for 5 minutes, and the supernatant was removed
437 and discarded. Nucleated cells were divided into two subsets, one for isolation of all $CD11B^+$ cells within
438 the bone marrow and the other for isolation of $CD11B^+/CD36^-$ and $CD11B^+/CD36^+$ cells. Cells were counted
439 and pelleted at 1000 rpm. Nucleated cells within the pellet were suspended in 100 µl MACS Buffer per
440 $1x10^7$. For isolation of $CD36^+$ cells, cells were then incubated with Allophycocyanin (APC)-conjugated anti-
441 CD36 (10 µl per $1x10^7$ cells, Miltenyi Biotech, #130-122-085) antibodies for 10 minutes at 4C. Cells were
442 pelleted, washed, suspended in 1X MACS buffer (80 µl per $1x10^7$ cells) and incubated with anti-APC
443 microbeads (20 µl per $1x10^7$ cells, Miltenyi Biotech, #130-090-855) for 15 minutes at 4C. Cells were
444 washed and then suspended in 500 µl MACS buffer. An LS MACS separation column was placed within
445 the magnetic field of a MACS Separator magnet and the column was equilibrated with 3 ml MACS buffer.
446 Following equilibration, anti-APC microbead-labeled cells were applied to the LS column. The column was
447 washed 3X with 3 ml MACS buffer. Unbound cells were used to isolate $CD11B^+CD36^-$ cells. To isolate APC-
448 labeled cells, the column was removed from the magnet and cells were flushed from the column with 5

449 ml 1X MACS buffer. Eluted cells were then pelleted at 1000 rpm for 5 minutes, and the supernatant was
450 removed and discarded. To isolate $CD11B^+$ cells from each of the three fractions (e.g., whole bone marrow,
451 $CD36^-$ cells, and $CD36^+$ cells), cells were then suspended in 100 µl 1X MACS Buffer per $1x10^7$ cells and
452 incubated with phycoerythrin (PE)-conjugated anti-CD11B (10 µl per $1x10^7$ cells, Miltenyi Biotech, #130-
453 113-235) for 10 minutes at 4C. Cells were washed, suspended in MACS buffer (80 µl per $1x10^7$ cells), and
454 incubated with anti-PE microbeads (20 µl per $1x10^7$ cells, Miltenyi Biotech, #130-048-801) for 15 minutes
455 at 4C. Magnetic sorting for PE-labeled cells was accomplished as described above. To validate effective
456 sorting of $CD36^+CD11B^+$ cells via MACS, flow cytometry was performed (n=3). For flow cytometry analysis,
457 we prepared single stained controls and double stained sample with unsorted nucleated cells with PE-
458 conjugated anti-CD11B, APC-conjugated anti-CD36, or co-stained with anti-CD11B and anti-CD36
459 antibodies ($1x10^6$ cells per condition), respectively. Data were acquired on a BD LSR II (H1010) and
460 analyses were performed using BD FACSDiva™ software.

461 *Culture of $CD36^+CD11B^+$ cells*

462 MACS sorted $CD11B^+$, $CD11B^+/CD36^-$ and $CD36^+/CD11B^+$ cells were isolated via MACS and cultured at a
463 density of density of $0.26x10^6$ per cm^2 in α-Minimal Essential Medium supplemented with 50 ng/ml
464 recombinant mouse macrophage-colony stimulating factor (M-CSF) (#416-ML, R&D Systems,
465 Minneapolis, MN, USA). Cells were maintained in culture and supplemented with M-CSF for 7 days or until
466 adherent. Medium conditioned by each cell fraction was then collected, filtered with a 70 µm filter to
467 remove cellular debris, and stored at -80C before subsequent analyses. Cells were lysed in TriZol reagent
468 (ThermoFisher Scientific, #15596018) for gene expression analyses. For osteoclastogenesis experiments,
469 cells from each fraction were plated at a density of $0.4x10^6/cm^2$ in αMEM supplemented with 90 ng/ml
470 RANKL (R&D Systems, #462-TR-010) and 50 ng/ml M-CSF. Cells were refed with αMEM supplemented
471 with RANKL and M-CSF every other day for seven days, fixed with 10% neutral buffered formalin, and
472 TRAP stained using the Leukocyte Acid Phosphatase (TRAP) kit (Sigma-Aldrich, #387A-1KT).

473 *RNA Isolation and Semi-quantitative RT-PCR*

474 Total RNA was extracted from human macrophages using TRIzol and chloroform. Reverse transcription
475 using the iScript™ Reverse Transcription Supermix (Biorad, #1708841) using 1 µg of total RNA was used to
476 generate cDNAs. Gene expression was then assessed via real-time PCR using gene-specific primers listed
477 in Table 1. Fold changes in gene expression for each sample were calculated using the $2^{-\Delta\Delta Ct}$ method
478 relative to control after normalization of gene-specific C_t values to Ywhaz C_t values (24, 42). Shown are
479 averaged data from three independent replicate experiments derived from female cultured cells.

480 **Table 1. Gene specific primers used for semi-quantitative RT-PCR.**

Target	Forward Primer	Reverse Primer
Wnt3a	5'-TGTTCTGGACAAAGCCACCC-3'	5'-AATGTCCTCACTACAGCCGC-3'
Wnt6	5'-ACTGGGGGTTCGAGAATGTC-3'	5'-TCTCTCGGATGTCCTGCTGC-3'
Wnt10b	5'-ACGCCGGGGAAGCGG-3'	5'-AGTCAGTCAGCGCCTCCAG-3'
Bmp1	5'-TGGCCATATCCAGTCTCCCA-3'	5'-TGTCGTGACGCTCAATCTCA-3'
Bmp2	5'-CTGCGGTCTCCTAAAGGTCG-3'	5'-ATGCTGAGCAGCCTCAACTC-3'

481

482 *Cortical Bone Defect Generation*

483 Single-cortex, fully stabilized, mid-diaphysis femoral defects were generated in the right femur as
484 previously described (24, 43). Mice in all experimental groups were given Buprenorphine SR provided
485 perioperatively at 0.5 mg/kg given 2-4 hours before surgery via subcutaneous injection. Mice were then
486 anesthetized with isoflurane and prepared for aseptic surgery. A small incision was made in the skin
487 overlying the right hamstring and the femoral bone shaft was exposed by blunt dissection of the
488 underlying muscle. A 0.7 mm diameter steel burr drill bit (#19007-07, Fine Science Tools, Foster City, CA)
489 and an electric drill was used to induce a single-cortex defect in the mid-diaphysis of the femur. Defects
490 were immediately irrigated with 1 ml sterile saline followed by incision closure. Mice were sacrificed by
491 carbon dioxide inhalation at postoperative day 14.

492 *Immunohistochemistry (IHC) and TRAP Staining*

493 Tibiae from 24-week-old female mice were collected, fixed in 10% neutral buffered formalin and then
494 stored in 70% ethanol. Following decalcification in 15% EDTA for 14 days, tissues were paraffin embedded
495 and 7 micron sections were collected. IHC staining was performed with antibodies directed to CD36
496 (#HPA002018, Sigma-Aldrich), or an irrelevant control. Detection was accomplished using the Mouse and
497 Rabbit Specific HRP/DAB (ABC) Detection IHC Kit (#ab64264, Abcam, Cabmbridge, UK). Sections were the
498 TRAP stained and then counterstained with Fast Green as previously described (42).

499 *BM-MSC Isolation and measurements of proliferation and osteoblastogenesis*

500 Bone marrow derived mesenchymal stems cells were isolated as previously described (44). Briefly, whole
501 bone marrow was flushed from the hind limbs of female C57Bl6/J mice. Red blood cells were lysed in 1X
502 RBC lysis buffer as described above. Nucleated cells were then pelleted and plated at a density of XXX in
503 10 cm plates. Cells were passaged five times to remove contaminating hematopoietic cells. Purity of
504 MSCs was assessed by flow cytometry with FITC-conjugated anti-CD90.2, anti-CD44, anti-Cd34, and anti-
505 Cd45 ($1x10^6$ cells per condition), respectively. Data were acquired on a BD LSR II (H1010) and analyses
506 were performed using BD FACSDiva™ software. MSCs were then cultured at a density of XXX cells/cm2 in
507 $CD11B^+$, $CD11B^+/CD36^-$ or $CD11B^+/CD36^+$ conditioned medium for 24 hours. MSC proliferation was then
508 determined using a Cck8 assay (Cell Counting Kit, Sigma Aldrich, #96992-100TESTS-F). To asses MSC
509 migration, transwell assays were performed using Conrning Costar transwell assay cell culture inserts
510 (Sigma Aldrich, #CLS3464-12EA). Before starting the assay, the transwell were equilibrated over night with
511 MEM (no FBS). Next day, ST2 cells were trypsinized and collected in 0.2% FBS containing MEM. A total of
512 $2x10^4$ cells were seeded into the upper chamber of the transwell inserts. The lower chamber was filled
513 with an equal mixture of conditioned medium and MEM (10% FBS). Then, the plate was incubated for
514 18hrs to allow migration. Following incubation, the plate was taken out and the media was removed. The
515 insert was washed with 1x PBS twice. The non-migrated cells were carefully removed from the upper side

516 of the membrane using cotton swab and the migrated cells on the other side of the membrane was fixed
517 with 100% methanol, for 5 min at room temperature and stained with Giemsa stain for 10min. Excess
518 stain was removed by washing the chamber with distilled water and air dried. The membrane was
519 carefully cut out using a scalpel blade and placed on slide. The membrane was mounted on the slide using
520 VECTASHIELD® Antifade Mounting Medium with DAPI. Cells were visualized under the fluorescent
521 microscope, and five random fields per insert were counted using Image J.

522 *Western Blotting*

523 Cell lysates were collected in a buffered SDS solution (0.1% glycerol, 0.01% SDS, 0.1 m Tris, pH 6.8) on ice.
524 Total protein concentrations were obtained with the Bio-Rad D_C assay (Bio-Rad). Proteins (20 µg) were
525 then resolved by SDS-PAGE and transferred to a polyvinylidene difluoride membrane. Western blotting
526 was performed with antibodies (1:2000 dilution) for WNT6 (Thermo Fisher Scientific, #24201-1-AP), Active
527 β-catenin (Millipore, #05-665-25UG), β-catenin (BD Biosciences, #610153), TCF1/7 (Cell Signaling
528 Technology, 2203T), phospho-JNK (Cell Signaling Technology, #4668T), JNK (Cell Signaling Technology,
529 #9252T), NFAT1 (Cell Signaling Technology, #4389S), Histone 3 (Millipore, #05-928), and corresponding
530 secondary antibodies conjugated to horseradish peroxidase (HRP) (Cell Signaling Technology). Antibody
531 binding was detected with the Supersignal West Femto Chemiluminescent Substrate (Pierce
532 Biotechnology, Rockford, IL). Shown are data from averaged from three males, but studies were
533 performed in females (n=3 per group) in three independent replicate experiments, each containing six
534 pooled replicate wells per group.

535 **CONFLICTS OF INTEREST**

536 The authors declare no conflict of interest.

537 **ACKNOWLEDGEMENTS**

538 The authors would like to thank the support from the Comparative Pathology Shared Resource, the
539 Minnesota Dental Research Center for Biomaterials and Biomechanics, and technical assistance from Mr.
540 David HH Molstad. This work was made possible by research grants from the National Institute for
541 Musculoskeletal, Arthritis, and Skin Diseases (R21AR084530), a seed grant from the UMN BIRCWH award
542 (HD055887), and the University of Minnesota Board of Regents. These contents are solely the
543 responsibility of the authors and do not necessarily represent the official views of the funding
544 organizations. The study was conducted according to the guidelines of the University of Minnesota
545 Institutional Animal Care and Use Committee (#2007-38247A approved on 08 August 2020). All data are
546 contained within this manuscript and are available from the corresponding author upon reasonable
547 request.

548 **REFERENCES**

549 1. Chevalley T, Rizzoli R. Acquisition of peak bone mass. Best Pract Res Clin Endocrinol Metab.
550 2022;36(2):101616.
551 2. Demontiero O, Vidal C, Duque G. Aging and bone loss: new insights for the clinician. Ther Adv
552 Musculoskelet Dis. 2012;4(2):61-76.
553 3. Sfeir JG, Drake MT, Khosla S, Farr JN. Skeletal Aging. Mayo Clin Proc. 2022;97(6):1194-208.
554 4. Wright NC, Looker AC, Saag KG, Curtis JR, Delzell ES, Randall S, et al. The recent prevalence of
555 osteoporosis and low bone mass in the United States based on bone mineral density at the femoral neck
556 or lumbar spine. J Bone Miner Res. 2014;29(11):2520-6.
557 5. Kannus P, Parkkari J, Niemi S, Palvanen M. Epidemiology of osteoporotic ankle fractures in elderly
558 persons in Finland. Ann Intern Med. 1996;125(12):975-8.
559 6. Leibson CL, Tosteson AN, Gabriel SE, Ransom JE, Melton LJ. Mortality, disability, and nursing home
560 use for persons with and without hip fracture: a population-based study. J Am Geriatr Soc.
561 2002;50(10):1644-50.
562 7. Magaziner J, Lydick E, Hawkes W, Fox KM, Zimmerman SI, Epstein RS, et al. Excess mortality
563 attributable to hip fracture in white women aged 70 years and older. Am J Public Health.
564 1997;87(10):1630-6.
565 8. Magaziner J, Simonsick EM, Kashner TM, Hebel JR, Kenzora JE. Predictors of functional recovery
566 one year following hospital discharge for hip fracture: a prospective study. J Gerontol. 1990;45(3):M101-
567 7.
568 9. Riggs BL, Melton LJ, 3rd. The worldwide problem of osteoporosis: insights afforded by
569 epidemiology. Bone. 1995;17(5 Suppl):505S-11S.
570 10. Clarke B. Normal bone anatomy and physiology. Clin J Am Soc Nephrol. 2008;3 Suppl 3(Suppl
571 3):S131-9.
572 11. Ramchand SK, Seeman E. The Influence of Cortical Porosity on the Strength of Bone During Growth
573 and Advancing Age. Curr Osteoporos Rep. 2018;16(5):561-72.

574 12. Cosman F, Crittenden DB, Ferrari S, Khan A, Lane NE, Lippuner K, et al. FRAME Study: The
575 Foundation Effect of Building Bone With 1 Year of Romosozumab Leads to Continued Lower Fracture Risk
576 After Transition to Denosumab. J Bone Miner Res. 2018;33(7):1219-26.
577 13. Graeff C, Campbell GM, Pena J, Borggrefe J, Padhi D, Kaufman A, et al. Administration of
578 romosozumab improves vertebral trabecular and cortical bone as assessed with quantitative computed
579 tomography and finite element analysis. Bone. 2015;81:364-9.
580 14. Weivoda MM, Bradley EW. Macrophages and Bone Remodeling. J Bone Miner Res.
581 2023;38(3):359-69.
582 15. Sims NA, Martin TJ. Osteoclasts Provide Coupling Signals to Osteoblast Lineage Cells Through
583 Multiple Mechanisms. Annu Rev Physiol. 2020;82:507-29.
584 16. Andreasen CM, El-Masri BM, MacDonald B, Laursen KS, Nielsen MH, Thomsen JS, et al. Local
585 coordination between intracortical bone remodeling and vascular development in human juvenile bone.
586 Bone. 2023;173:116787.
587 17. Liu B, Salgado OC, Singh S, Hippen KL, Maynard JC, Burlingame AL, et al. The lineage stability and
588 suppressive program of regulatory T cells require protein O-GlcNAcylation. Nat Commun. 2019;10(1):354.
589 18. Wang H, Breed ER, Lee YJ, Qian LJ, Jameson SC, Hogquist KA. Myeloid cells activate iNKT cells to
590 produce IL-4 in the thymic medulla. Proc Natl Acad Sci U S A. 2019;116(44):22262-8.
591 19. Wang H, Hogquist KA. CCR7 defines a precursor for murine iNKT cells in thymus and periphery.
592 Elife. 2018;7.
593 20. Faltusova K, Chen CL, Heizer T, Bajecny M, Szikszai K, Paral P, et al. Altered Erythro-Myeloid
594 Progenitor Cells Are Highly Expanded in Intensively Regenerating Hematopoiesis. Front Cell Dev Biol.
595 2020;8:98.
596 21. Mohamad SF, Gunawan A, Blosser R, Childress P, Aguilar-Perez A, Ghosh J, et al. Neonatal
597 Osteomacs and Bone Marrow Macrophages Differ in Phenotypic Marker Expression and Function. J Bone
598 Miner Res. 2021;36(8):1580-93.
599 22. McDonald MM, Khoo WH, Ng PY, Xiao Y, Zamerli J, Thatcher P, et al. Osteoclasts recycle via
600 osteomorphs during RANKL-stimulated bone resorption. Cell. 2021;184(5):1330-47 e13.
601 23. Isojima T, Sims NA. Cortical bone development, maintenance and porosity: genetic alterations in
602 humans and mice influencing chondrocytes, osteoclasts, osteoblasts and osteocytes. Cell Mol Life Sci.
603 2021;78(15):5755-73.
604 24. Molstad DHH, Zars E, Norton A, Mansky KC, Westendorf JJ, Bradley EW. Hdac3 deletion in myeloid
605 progenitor cells enhances bone healing in females and limits osteoclast fusion via Pmepa1. Sci Rep.
606 2020;10(1):21804.
607 25. Helming L, Winter J, Gordon S. The scavenger receptor CD36 plays a role in cytokine-induced
608 macrophage fusion. J Cell Sci. 2009;122(Pt 4):453-9.
609 26. Ambrosi TH, Marecic O, McArdle A, Sinha R, Gulati GS, Tong X, et al. Aged skeletal stem cells
610 generate an inflammatory degenerative niche. Nature. 2021;597(7875):256-62.
611 27. Ucer S, Iyer S, Kim HN, Han L, Rutlen C, Allison K, et al. The Effects of Aging and Sex Steroid
612 Deficiency on the Murine Skeleton Are Independent and Mechanistically Distinct. J Bone Miner Res.
613 2017;32(3):560-74.
614 28. Yahara Y, Ma X, Gracia L, Alman BA. Monocyte/Macrophage Lineage Cells From Fetal
615 Erythromyeloid Progenitors Orchestrate Bone Remodeling and Repair. Front Cell Dev Biol. 2021;9:622035.
616 29. Askmyr MK, Fasth A, Richter J. Towards a better understanding and new therapeutics of
617 osteopetrosis. Br J Haematol. 2008;140(6):597-609.
618 30. Jacome-Galarza CE, Percin GI, Muller JT, Mass E, Lazarov T, Eitler J, et al. Developmental origin,
619 functional maintenance and genetic rescue of osteoclasts. Nature. 2019;568(7753):541-5.
620 31. Novak S, Roeder E, Kalinowski J, Jastrzebski S, Aguila HL, Lee SK, et al. Osteoclasts Derive
621 Predominantly from Bone Marrow-Resident CX3CR1(+) Precursor Cells in Homeostasis, whereas

622 Circulating CX3CR1(+) Cells Contribute to Osteoclast Development during Fracture Repair. J Immunol.
623 2020;204(4):868-78.
624 32. Xia Y, Inoue K, Du Y, Baker SJ, Premkumar Reddy E, Greenblatt MB, et al. TGFbeta reprograms TNF
625 stimulation of macrophages towards a non-canonical pathway driving inflammatory osteoclastogenesis.
626 Nat Commun. 2022;13(1):3920.
627 33. Yahara Y, Barrientos T, Tang YJ, Puviindran V, Nadesan P, Zhang H, et al. Erythromyeloid
628 progenitors give rise to a population of osteoclasts that contribute to bone homeostasis and repair. Nat
629 Cell Biol. 2020;22(1):49-59.
630 34. Kevorkova O, Martineau C, Martin-Falstrault L, Sanchez-Dardon J, Brissette L, Moreau R. Low-
631 bone-mass phenotype of deficient mice for the cluster of differentiation 36 (CD36). PLoS One.
632 2013;8(10):e77701.
633 35. Koduru SV, Sun BH, Walker JM, Zhu M, Simpson C, Dhodapkar M, et al. The contribution of cross-
634 talk between the cell-surface proteins CD36 and CD47-TSP-1 in osteoclast formation and function. J Biol
635 Chem. 2018;293(39):15055-69.
636 36. Weivoda MM, Ruan M, Hachfeld CM, Pederson L, Howe A, Davey RA, et al. Wnt Signaling Inhibits
637 Osteoclast Differentiation by Activating Canonical and Noncanonical cAMP/PKA Pathways. J Bone Miner
638 Res. 2016;31(1):65-75.
639 37. Glass DA, 2nd, Bialek P, Ahn JD, Starbuck M, Patel MS, Clevers H, et al. Canonical Wnt signaling in
640 differentiated osteoblasts controls osteoclast differentiation. Dev Cell. 2005;8(5):751-64.
641 38. Andersen TL, Sondergaard TE, Skorzynska KE, Dagnaes-Hansen F, Plesner TL, Hauge EM, et al. A
642 physical mechanism for coupling bone resorption and formation in adult human bone. Am J Pathol.
643 2009;174(1):239-47.
644 39. Eriksen EF, Gundersen HJ, Melsen F, Mosekilde L. Reconstruction of the formative site in iliac
645 trabecular bone in 20 normal individuals employing a kinetic model for matrix and mineral apposition.
646 Metab Bone Dis Relat Res. 1984;5(5):243-52.
647 40. Lassen NE, Andersen TL, Ploen GG, Soe K, Hauge EM, Harving S, et al. Coupling of Bone Resorption
648 and Formation in Real Time: New Knowledge Gained From Human Haversian BMUs. J Bone Miner Res.
649 2017;32(7):1395-405.
650 41. Bouxsein ML, Boyd SK, Christiansen BA, Guldberg RE, Jepsen KJ, Muller R. Guidelines for
651 assessment of bone microstructure in rodents using micro-computed tomography. J Bone Miner Res.
652 2010;25(7):1468-86.
653 42. Mattson AM, Begun DL, Molstad DHH, Meyer MA, Oursler MJ, Westendorf JJ, et al. Deficiency in
654 the phosphatase PHLPP1 suppresses osteoclast-mediated bone resorption and enhances bone formation
655 in mice. J Biol Chem. 2019;294(31):11772-84.
656 43. McGee-Lawrence ME, Razidlo DF. Induction of fully stabilized cortical bone defects to study
657 intramembranous bone regeneration. Methods Mol Biol. 2015;1226:183-92.
658 44. Jung JP, Bache-Wiig MK, Provenzano PP, Ogle BM. Heterogeneous Differentiation of Human
659 Mesenchymal Stem Cells in 3D Extracellular Matrix Composites. Biores Open Access. 2016;5(1):37-48.

660

661 **Figure Legends**

662 **Figure 1. Generation of Bone Marrow Chimeric Mice.** (A-E) Young male recipient mice were lethally
663 irradiated and reconstituted with T cell-depleted bone marrow (BM) from 1) young male, 2) aged male,
664 3) young female, or 4) aged female donor mice. Recipient mice were aged to 24-weeks for subsequent
665 analyses. (A) Experimental overview. (B) RNA was collected from BM and livers of chimeric mice in group
666 3 and expression of X- and Y-linked genes was determined via qPCR, *p<0.05, n=8. (C-E) Chimeric mice
667 in each group were collected six months post-BM transplantation. Mice were (C) photographed. (D) Body
668 and (E) spleen weight/body weight was assessed, *p<0.05. Groups: 1: young male BM, n=10; 2: aged male
669 BM, n=8, 3: young female BM, n=8; and 4: aged female BM, n=8

670 **Figure 2. Transplantation of Aged Bone Marrow Enhances Cortical Bone.** (A-G) Young male recipient mice
671 were lethally irradiated and reconstituted with T cell-depleted bone marrow (BM) from 1) young male, 2)
672 aged male, 3) young female, or 4) aged female donor mice. Recipient mice were aged to 24-weeks for
673 subsequent analyses. Non-irradiated 24-week-old males were used for comparisons. Micro-CT of the
674 femoral mid-shaft was performed to determine (A) cortical BV/TV, (B) cortical thickness, (C) endosteal
675 perimeter (Pm) and (D) reconstructions were generated. The distal femoral region was also assesse to
676 determine trabecular (E) BV/TV, (F) trabecular spacing, and (G) trabecular thickness. #p< 0.05 NI vs group
677 1, *p<0.05 vs. group 1. Groups: NI: non-irradiated control, n=10; 1: young male BM, n=10; 2: aged male
678 BM, n=8, 3: young female BM, n=8; and 4: aged female BM, n=8

679 **Figure 3. Identification of Anabolic Bone Marrow Subsets.** (A-R) Young male recipient mice were lethally
680 irradiated and reconstituted with T cell-depleted bone marrow (BM) from 1) young male or 2) aged male
681 donor mice. Recipient mice were aged to 24-weeks for subsequent analyses. $CD11B^+$ cells were collected
682 from mice in groups 1 and 2 above and scRNA-Seq was performed using 10X Genomics technology.
683 Resulting data were integrated and comparative analyses were performed. (A) UMAP 2D representation
684 of $CD11B^+$ clusters derived from recipient mice transplanted with aged and young bone marrow. (B-Q)

685 Expression of surface markers used to differentiate clusters. (R) Heatmap of top differentially expressed
686 genes from mice in group 2 vs 1 in clusters 14-16 across all clusters.

687 **Figure 4. Identification of Anabolic Bone Marrow Subsets.** (A-S) Young male recipient mice were lethally
688 irradiated and reconstituted with T cell-depleted bone marrow (BM) from 1) young female or 2) aged
689 female donor mice. Recipient mice were aged to 24-weeks for subsequent analyses. $CD11B^+$ cells were
690 collected from mice in groups 1 and 2 above and scRNA-Seq was performed using 10X Genomics
691 technology. Resulting data were integrated and comparative analyses were performed. (A) UMAP 2D
692 representation of $CD11B^+$ clusters derived from recipient mice transplanted with aged and young bone
693 marrow. (B-Q) Expression of surface markers used to differentiate clusters. (R) Heatmap of top
694 differentially expressed genes from mice in group 2 vs 1 in clusters 14-16 across all clusters.

695 **Figure 5. Single cell RNA-Seq of $CD11B^+$ cells from male and female bone marrow reveals subsets of**
696 **myeloid cells in aged myeloid cells that express anabolic cytokines.** (A-H) $CD11B^+$ cells from the bone
697 marrow of 8- or 40-week-old male and female mice were collected and single cell RNA-Seq was
698 performed. (A) UMPA representation of data obtained from 8-week-old males. (B) Heatmap and
699 hierarchical clustering of differentially expressed genes from clusters yielded from 8-week-old male data.
700 (C) UMPA representation of data obtained from 8-week-old females. (D) Heatmap and hierarchical
701 clustering of differentially expressed genes from clusters yielded from 8-week-old female data. (E) UMAP
702 representation of data obtained from 40-week-old males. (F) Heatmap and hierarchical clustering of
703 differentially expressed genes from clusters yielded from 40-week-old male data. (G) UMPA
704 representation of data obtained from 40-week-old females. (H) Heatmap and hierarchical clustering of
705 differentially expressed genes from clusters yielded from 40-week-old female data.

706 **Figure 6. $CD36^+$ cells associate with sites of cortical bone regeneration, but are not osteoclast**
707 **progenitors**. (A) Immunohistochemical staining for CD36 of paraffin sections from uninjured 12-week-old

708 females (upper panels) or cortical bone defects (lower panels). Sections are counterstained with TRAP
709 (purple) and fast green (n=5/group). BM: bone marrow, CB: cortical bone, OC: osteoclast (B) $CD11B^{+}CD36^{-}$
710 and $CD11B^{+}CD36^{+}$ BM cells were isolated and cultured in the presence of RANKL and M-CSF. TRAP staining
711 was performed on day 4 (n=3).

712 **Figure 7. $CD11B^{+}CD36^{+}$ Cells Promote Bone Formation CD11B+CD36+ cell promote bone formation.** (A)
713 Flow cytometry. CD11b+CD36- and CD11b+CD36+ cells were sorted and gene expression was evaluated
714 by qPCR (B-F) and western blotting (G), n=3, *p* values as shown. (H) Experimental design for (I-Q)
715 Oseoprogenitor cells were treated with CM for 24 hours and (I) Cck8 and (J) transwell assays were
716 performed. (K-Q)) Osteoprogenitor cells were treated with CM for 8 weeks and Alizarin Red staining (K)
717 was performed and quantified (L), n=3, p values as shown. RNA was collected and gene expression (M-Q)
718 was assessed by qPCR, n=3 , p values as shown. (R) Osteoprogenitor cells were treated with CM for 60
719 minutes and western blotting was performed (n=3).

720 **Figure 8. $CD36^{+}$ Cells Associate with Sites of Bone Remodeling. Figure 9. Identification of human BM**
721 **macrophage subsets.** $CD11B^{+}$ cells were collected from the BM aspirate of a 45-year-old female and
722 scRNA-Seq was performed using 10X Genomics technology. (A) UMAP 2D representation of $CD11B^{+}$
723 clusters. (B-Q) Expression of surface markers used to differentiate clusters. Violin plots of CD36 (R) and
724 Wnt6 (S) expression.

725

Figure 1

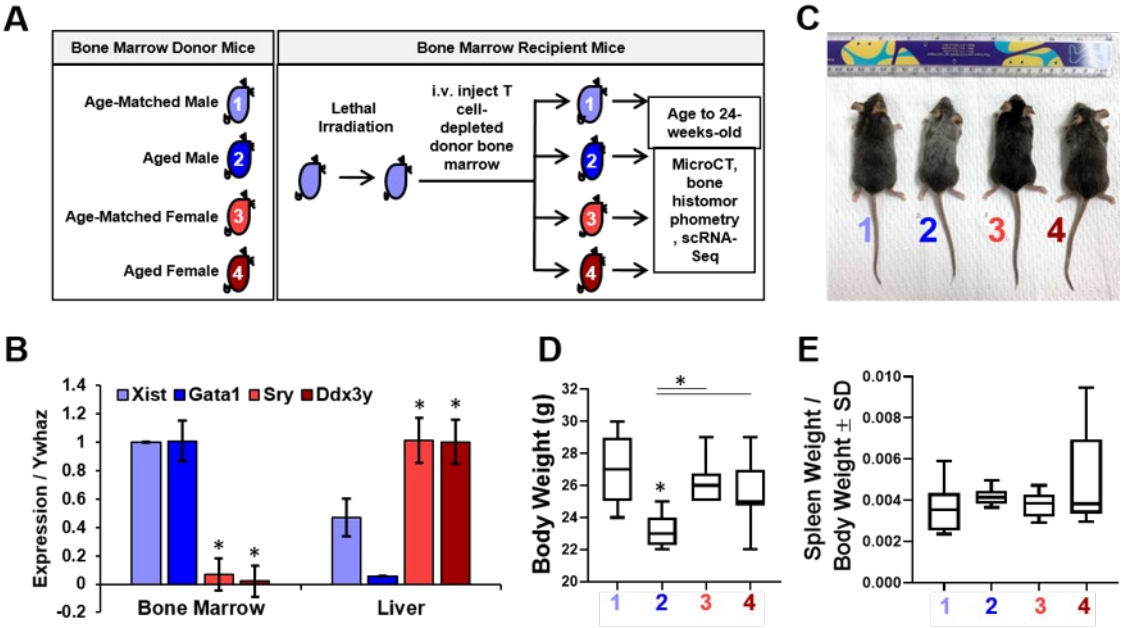
A
Bone Marrow Donor Mice
Bone Marrow Recipient Mice
Age-Matched Male
Aged Male
Age-Matched Female
Aged Female
Lethal Irradiation
i.v. inject T cell-depleted donor bone marrow
Age to 24-weeks-old
MicroCT, bone histomorphometry, scRNA-Seq
C
1
2
3
4
B
Xist
Gata1
Sry
Ddx3y
Expression / Ywhaz
Bone Marrow
Liver
D
Body Weight (g)
E
Spleen Weight / Body Weight ± SD

Figure 2

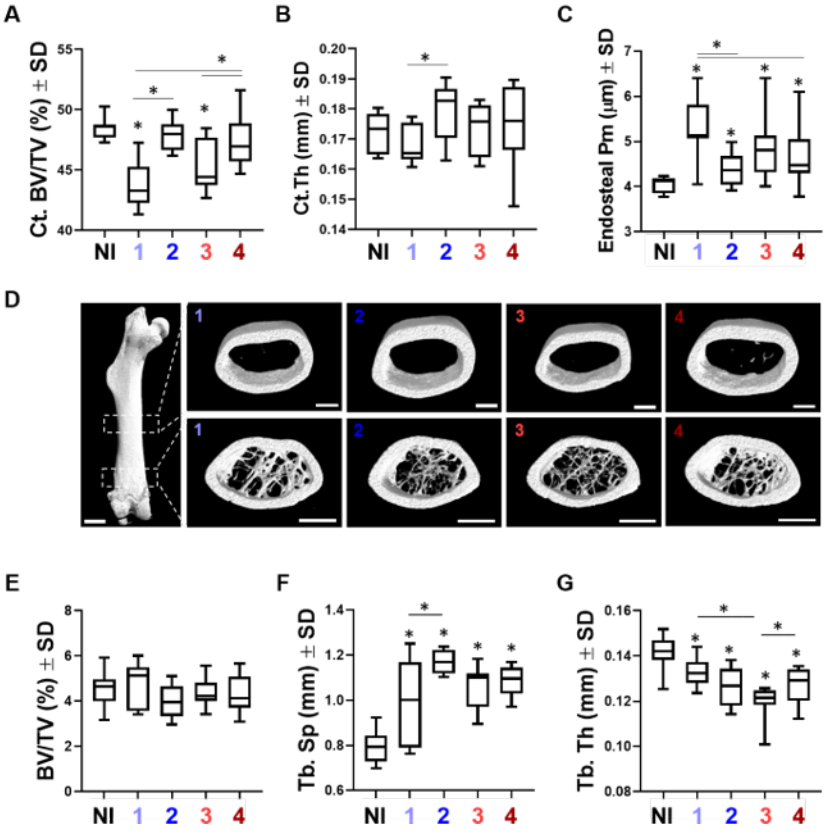
A
Ct. BV/TV (%) ± SD
B
Ct.Th (mm) ± SD
C
Endosteal Pm (µm) ± SD
D
E
BV/TV (%) ± SD
F
Tb. Sp (mm) ± SD
G
Tb. Th (mm) ± SD
NI 1 2 3 4

Figure 3

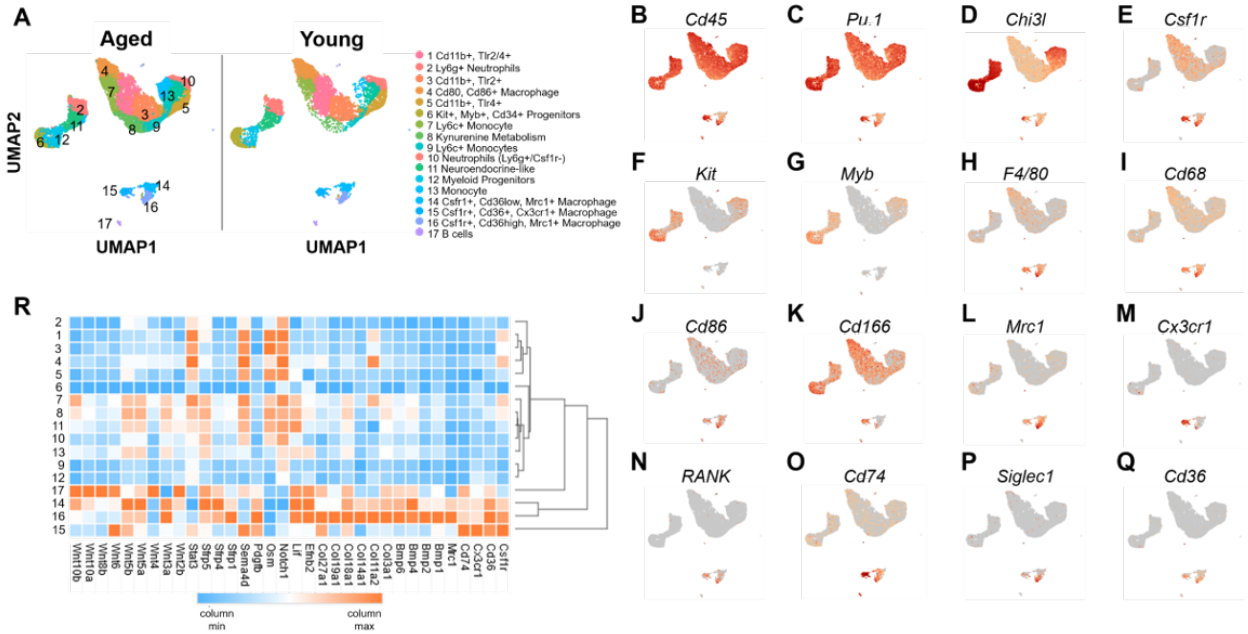
A
Aged
Young
UMAP2
UMAP1
UMAP1
1 Cd11b+, Tlr2/4+
2 Ly6g+ Neutrophils
3 Cd11b+, Tlr2+
4 Cd80, Cd86+ Macrophage
5 Cd11b+, Tlr4+
6 Kit+, Myb+, Cd34+ Progenitors
7 Ly6c+ Monocyte
8 Kynurenine Metabolism
9 Ly6c+ Monocytes
10 Neutrophils (Ly6g+/Csf1r-)
11 Neuroendocrine-like
12 Myeloid Progenitors
13 Monocyte
14 Csfr1+, Cd36low, Mrc1+ Macrophage
15 Csf1r+, Cd36+, Cx3cr1+ Macrophage
16 Csf1r+, Cd36high, Mrc1+ Macrophage
17 B cells
B Cd45
C Pu.1
D Chi3l
E Csf1r
F Kit
G Myb
H F4/80
I Cd68
J Cd86
K Cd166
L Mrc1
M Cx3cr1
N RANK
O Cd74
P Siglec1
Q Cd36
R
column min
column max

Figure 4

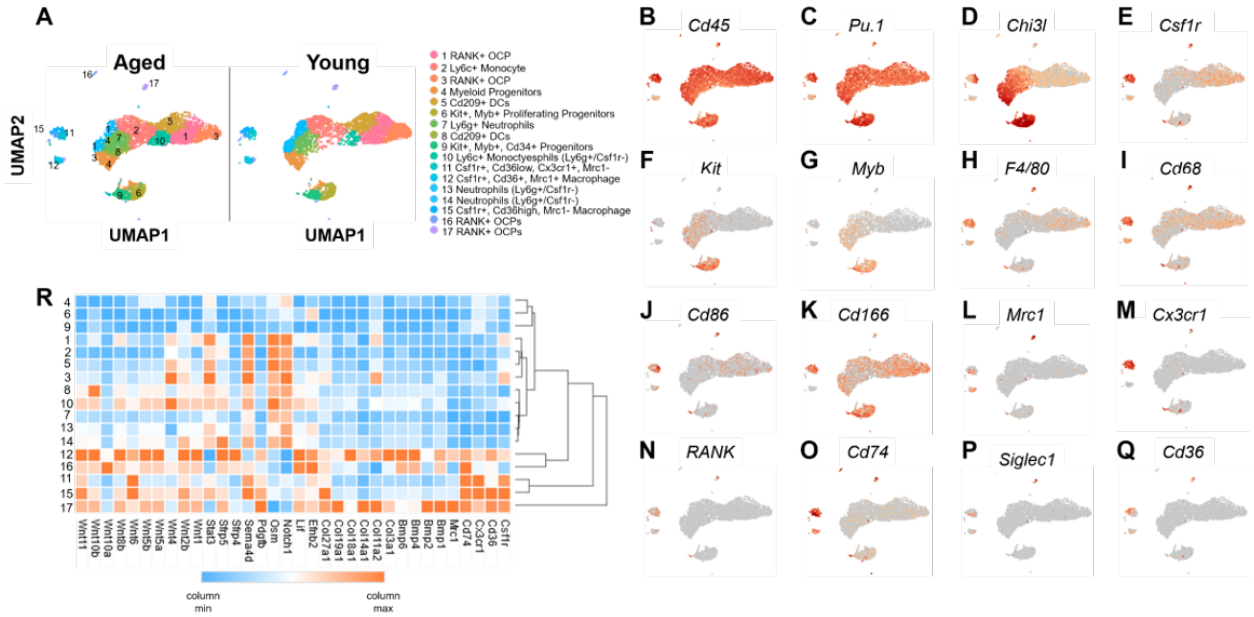
A
Aged
Young
UMAP2
UMAP1
UMAP1
1 RANK+ OCP
2 Ly6c+ Monocyte
3 RANK+ OCP
4 Myeloid Progenitors
5 Cd209+ DCs
6 Kit+, Myb+ Proliferating Progenitors
7 Ly6g+ Neutrophils
8 Cd209+ DCs
9 Kit+, Myb+, Cd34+ Progenitors
10 Ly6c+ Monoctyesphils (Ly6g+/Csf1r-)
11 Csf1r+, Cd36low, Cx3cr1+, Mrc1-
12 Csf1r+, Cd36+, Mrc1+ Macrophage
13 Neutrophils (Ly6g+/Csf1r-)
14 Neutrophils (Ly6g+/Csf1r-)
15 Csf1r+, Cd36high, Mrc1- Macrophage
16 RANK+ OCPs
17 RANK+ OCPs
B Cd45
C Pu.1
D Chi3l
E Csf1r
F Kit
G Myb
H F4/80
I Cd68
J Cd86
K Cd166
L Mrc1
M Cx3cr1
N RANK
O Cd74
P Siglec1
Q Cd36
R
Wnt11
Wnt10b
Wnt10a
Wnt8b
Wnt6
Wnt5b
Wnt5a
Wnt4
Wnt2b
Wnt1
Stat3
Stfp5
Stfp4
Sema4d
Pdgfb
Osm
Notch1
Lif
Efnb2
Col27a1
Col19a1
Col18a1
Col14a1
Col11a2
Col3a1
Bmp6
Bmp4
Bmp2
Bmp1
Mrc1
Cd74
Cx3cr1
Cd36
Csf1r
column min
column max

Figure 5

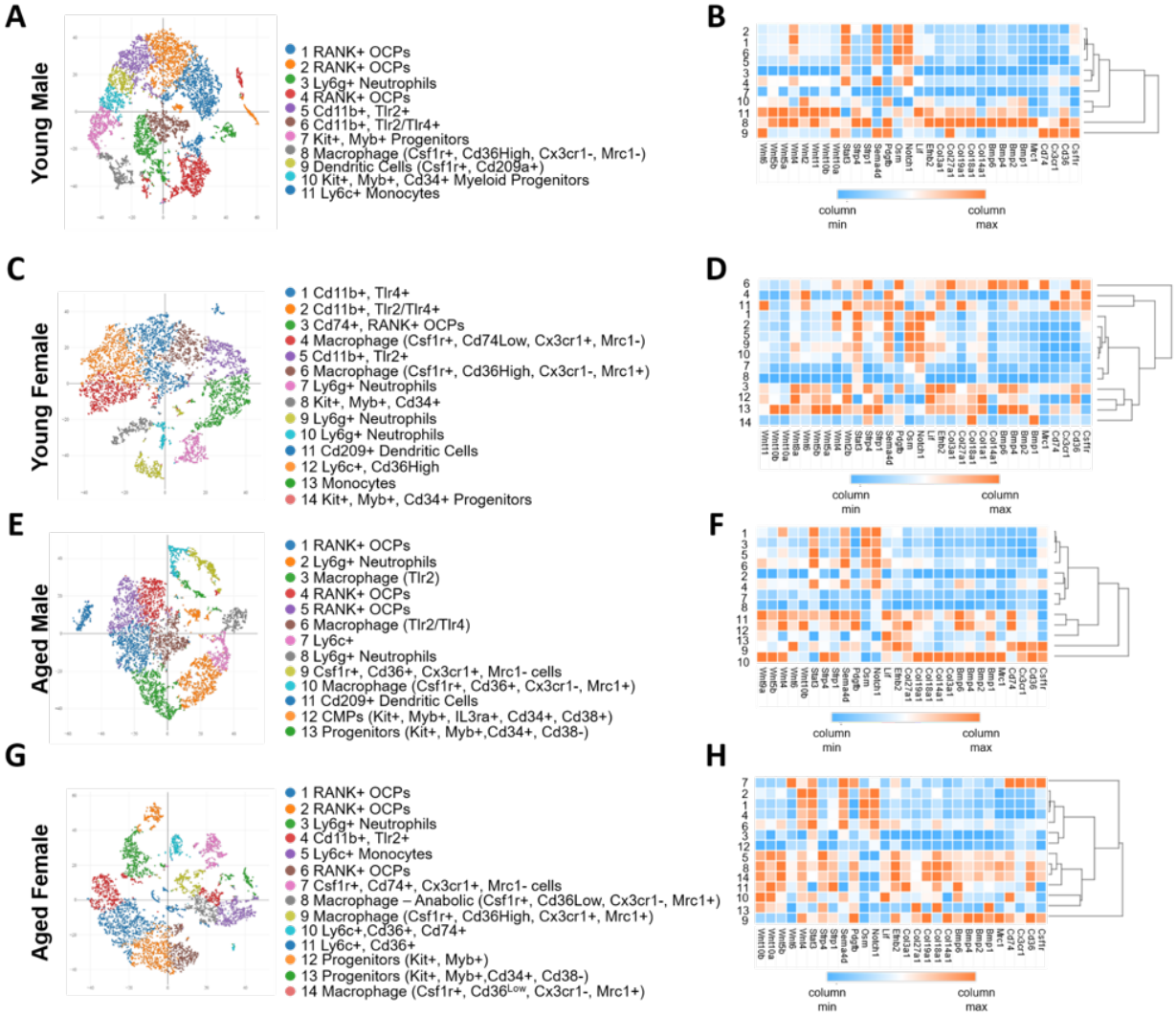
A
Young Male
1 RANK+ OCPs
2 RANK+ OCPs
3 Ly6g+ Neutrophils
4 RANK+ OCPs
5 Cd11b+, Tlr2+
6 Cd11b+, Tlr2/Tlr4+
7 Kit+, Myb+ Progenitors
8 Macrophage (Csf1r+, Cd36High, Cx3cr1-, Mrc1-)
9 Dendritic Cells (Csf1r+, Cd209a+)
10 Kit+, Myb+, Cd34+ Myeloid Progenitors
11 Ly6c+ Monocytes
B
column min
column max
C
Young Female
1 Cd11b+, Tlr4+
2 Cd11b+, Tlr2/Tlr4+
3 Cd74+, RANK+ OCPs
4 Macrophage (Csf1r+, Cd74Low, Cx3cr1+, Mrc1-)
5 Cd11b+, Tlr2+
6 Macrophage (Csf1r+, Cd36High, Cx3cr1-, Mrc1+)
7 Ly6g+ Neutrophils
8 Kit+, Myb+, Cd34+
9 Ly6g+ Neutrophils
10 Ly6g+ Neutrophils
11 Cd209+ Dendritic Cells
12 Ly6c+, Cd36High
13 Monocytes
14 Kit+, Myb+, Cd34+ Progenitors
D
column min
column max
E
Aged Male
1 RANK+ OCPs
2 Ly6g+ Neutrophils
3 Macrophage (Tlr2)
4 RANK+ OCPs
5 RANK+ OCPs
6 Macrophage (Tlr2/Tlr4)
7 Ly6c+
8 Ly6g+ Neutrophils
9 Csf1r+, Cd36+, Cx3cr1+, Mrc1- cells
10 Macrophage (Csf1r+, Cd36+, Cx3cr1-, Mrc1+)
11 Cd209+ Dendritic Cells
12 CMPs (Kit+, Myb+, IL3ra+, Cd34+, Cd38+)
13 Progenitors (Kit+, Myb+,Cd34+, Cd38-)
F
column min
column max
G
Aged Female
1 RANK+ OCPs
2 RANK+ OCPs
3 Ly6g+ Neutrophils
4 Cd11b+, Tlr2+
5 Ly6c+ Monocytes
6 RANK+ OCPs
7 Csf1r+, Cd74+, Cx3cr1+, Mrc1- cells
8 Macrophage – Anabolic (Csf1r+, Cd36Low, Cx3cr1-, Mrc1+)
9 Macrophage (Csf1r+, Cd36High, Cx3cr1+, Mrc1+)
10 Ly6c+,Cd36+, Cd74+
11 Ly6c+, Cd36+
12 Progenitors (Kit+, Myb+)
13 Progenitors (Kit+, Myb+,Cd34+, Cd38-)
14 Macrophage (Csf1r+, Cd36Low, Cx3cr1-, Mrc1+)
H
column min
column max

741 **Figure 6**

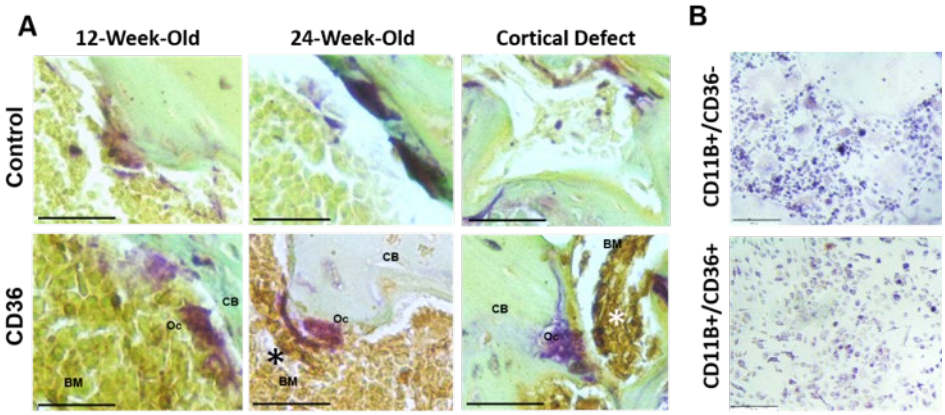

742

743

744

Figure 7

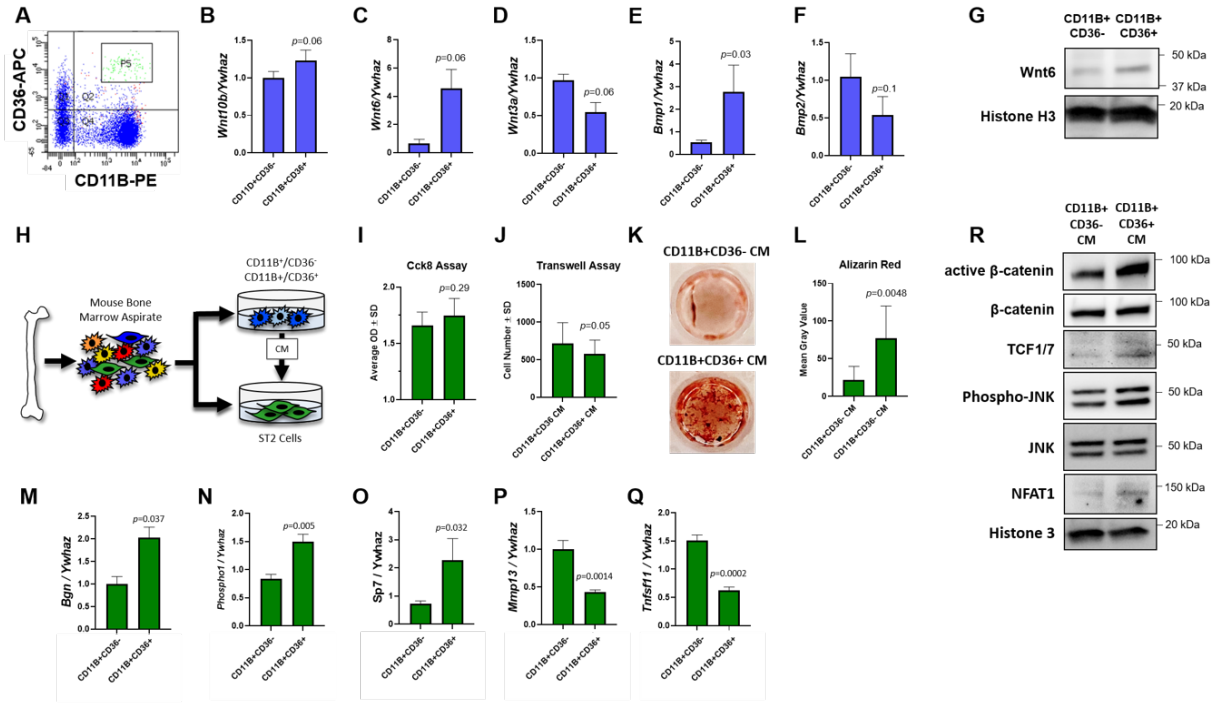

745

746

Figure 8

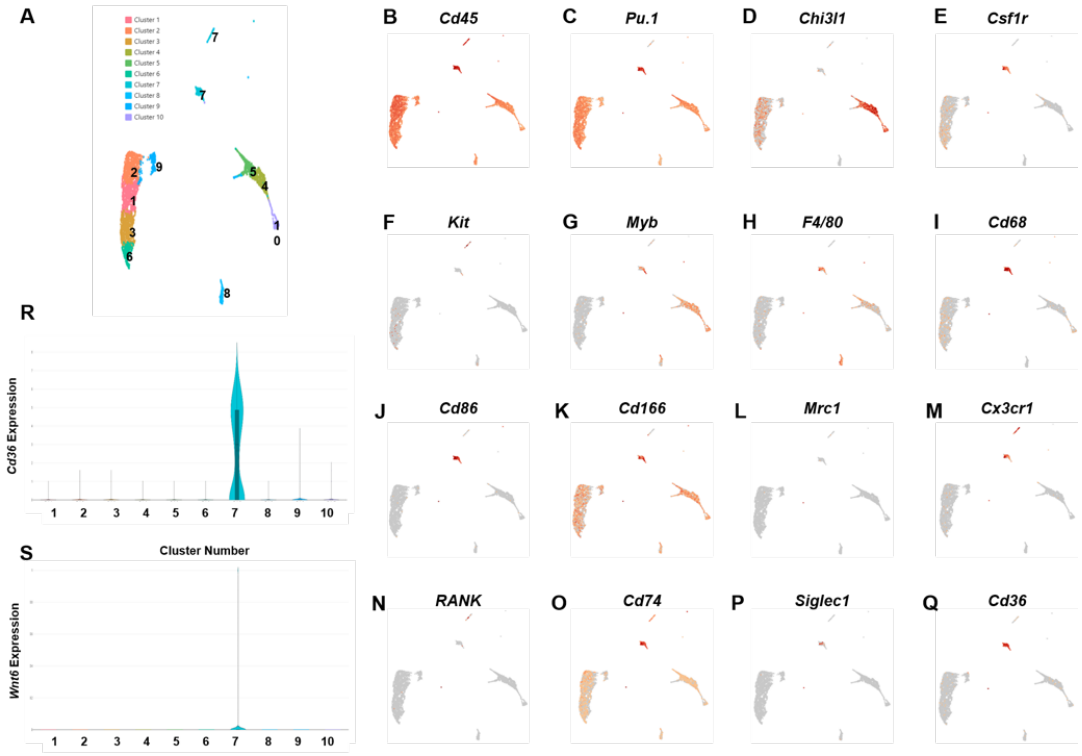
A
B Cd45
C Pu.1
D Chi3l1
E Csf1r
F Kit
G Myb
H F4/80
I Cd68
J Cd86
K Cd166
L Mrc1
M Cx3cr1
N RANK
O Cd74
P Siglec1
Q Cd36
R
Cd36 Expression
S
Cluster Number
Wnt6 Expression